TENTH AUSTRALASIAN FLUID MECHANICS
CONFERENCE - UNIVERSITY OF MELBOURNE
11-15 DECEMBER 1989

Keynote paper KS-3

VORTICITY GENERATION AND TRANSPORT

Hans HORNUNG

Graduate Aeronautical Laboratories
California Institute of Technology
Pasadena, California 91125
USA

ABSTRACT

The formula derived by Lighthill (1967) and extended by Morton (1984), as well as others, for the source strength of vorticity at a wall is shown to be largely independent of the material properties of the fluid. Previous derivations assume the fluid to be Newtonian.

The rules governing the configuration of the integral curves of the direction field of vorticity transport in a flow field are established. Examples are used to illustrate the features of these vorticity transport lines.

Examples are used also to illustrate how vorticity may be generated within a flow field by effects due to material properties such as compressibility.

1. INTRODUCTION

The idea of determining an expression for the vorticity source at a wall is not new. In particular, Lighthill obtained the source strength at a wall by applying the no-slip condition and assuming the flow to be at constant density and Newtonian. Morton extended this work to more general cases, and Wu et al. (1987) included further three-dimensional and compressibility effects in their expression. Specifically, Morton's expression (in the present notation) for the source strength is

$$\underset{\approx}{J}_0 \cdot \hat{\underset{\sim}{n}} = -\hat{\underset{\sim}{n}} \times \left[\frac{d\underset{\sim}{v}_0}{dt} + \frac{1}{\rho_0} (grad\, p)_0 \right], \qquad (1)$$

where $\underset{\sim}{v}_0$ is the velocity of the (non-rotating) plane wall with unit normal vector $\hat{\underset{\sim}{n}}$, and ρ_0 and p_0 are density and pressure at the wall.

All previous work derives the source strength from the expression for the diffusive vorticity flux of a Newtonian fluid. The resulting expression does not, however, contain the parameter of this material behavior (the kinematic viscosity), but only the dynamical boundary conditions at the wall. This is a strong indication for the possibility that the form of this expression is independent of material properties. This point is addressed in section 2.

In section 3 the direction field of vorticity transport is considered in the simple case of plane flow at constant density. Finally, section 4 gives examples of vorticity generation by a vortex near a wall, a mechanism important in turbulence, and two examples of vorticity generation by the baroclinic torque in steady and unsteady compressible flows.

2. THE VORTICITY SOURCE STRENGTH AT A SOLID BOUNDARY

Consider a body of fluid in an inertial frame. Let the coordinates of a material element of fluid in this frame be $\underset{\sim}{x}$. The velocity field is $\underset{\sim}{v}(\underset{\sim}{x},t)$, where t is time. The vorticity $\underset{\sim}{\omega}(\underset{\sim}{x},t)$ defined as curl $\underset{\sim}{v}$. It is twice the angular velocity of the material element.

Introduce a quantity $\underset{\sim}{Q}$, of which the vorticity is the density. I.e., vorticity is $\underset{\sim}{Q}$ per unit volume. $\underset{\sim}{Q}$ is a measure of specific angular momentum, i.e., of angular momentum per unit mass. Now consider a tensor quantity $\underset{\approx}{J}$, for which

$$\frac{D\underset{\sim}{\omega}}{Dt} = -div\, \underset{\approx}{J}. \qquad (2)$$

This equation defines $\underset{\approx}{J}$ as the transport per unit time across unit area of the quantity $\underset{\sim}{Q}$. $\underset{\approx}{J}$ has the dimensions of acceleration and is a measure of the rate of transfer of specific angular momentum per unit area. It is therefore proportional to the torque applied at that area.

Let the fluid be bounded by a solid wall normal to the z-axis of a Cartesian frame. The torque exerted by the wall on an element of fluid is the curl of the force exerted by the wall on the element. Per unit wall area this force may be written as $\underset{\approx}{S}_0 \cdot \hat{\underset{\sim}{k}}$, where $\underset{\approx}{S}_0$ is the stress at the wall and $\hat{\underset{\sim}{k}}$ is the unit vector normal to the wall. Therefore,

$$\underset{\approx}{J}_0 = \frac{1}{\rho_0} curl\, (\underset{\approx}{S}_0 \cdot \hat{\underset{\sim}{k}}) \qquad (3)$$

is a measure of the transport of specific angular momentum per unit area and time across the wall. The subscript signifies pertinence to the wall.

In order to examine the right hand side of this expression, write the stress as

$$\underset{\approx}{S} = \underset{\approx}{R} - \underset{\approx}{I} p, \qquad (4)$$

where $(-p)$ is the isotropic part of the normal stress (p is the pressure), $\underset{\approx}{I}$ is unit tensor, and $\underset{\approx}{R}$ is the frictional stress. $\underset{\approx}{R}$ contains the tangential stress elements denoted with the symbol τ, as well as the anisotropic part of the normal stress, which leads to normal stress differences denoted by the symbol σ. Thus,

$$\underset{\approx}{S} = \underset{\approx}{R} - \underset{\approx}{I} p,$$

$$= \begin{bmatrix} -p & \tau_{xy} & \tau_{xz} \\ \tau_{xy} & \sigma_1 - p & \tau_{yz} \\ \tau_{xz} & \tau_{yz} & \sigma_2 - p \end{bmatrix}. \qquad (5)$$

Hence

$$curl\,(\underset{\approx}{S}_0\cdot\hat{\underset{\sim}{k}}) = curl\left[\begin{bmatrix}\tau_{xz}\\ \tau_{yz}\\ \sigma_2-p\end{bmatrix}_0\right]$$

$$= \begin{bmatrix}\dfrac{\partial(\sigma_2-p)}{\partial y}-\dfrac{\partial\tau_{yz}}{\partial z}\\ \dfrac{\partial\tau_{xz}}{\partial z}-\dfrac{\partial(\sigma_2-p)}{\partial x}\\ \dfrac{\partial\tau_{yz}}{\partial x}-\dfrac{\partial\tau_{xz}}{\partial y}\end{bmatrix}_0 \qquad (6)$$

This may be related to the momentum equation, which, at the wall, becomes

$$\rho_0\frac{d\underset{\sim}{v}_0}{dt} = div\underset{\approx}{S}_0 = \begin{bmatrix}-\dfrac{\partial p}{\partial x}\\ \dfrac{\partial(\sigma_1-p)}{\partial y}\\ \dfrac{\partial(\sigma_2-p)}{\partial z}\end{bmatrix}_0 + \begin{bmatrix}\dfrac{\partial\tau_{xy}}{\partial y}+\dfrac{\partial\tau_{xz}}{\partial z}\\ \dfrac{\partial\tau_{xy}}{\partial x}+\dfrac{\partial\tau_{yz}}{\partial z}\\ \dfrac{\partial\tau_{xz}}{\partial x}+\dfrac{\partial\tau_{yz}}{\partial y}\end{bmatrix}_0, \qquad (7)$$

when the no-slip condition is applied and body forces are excluded. $d\underset{\sim}{v}_0/dt$ is the acceleration of the wall. This may be further simplified for a rigid wall, because the strain rates leading to the terms $\partial\tau_{xy}/\partial y$ and $\partial\tau_{xy}/\partial x$ are then identically zero on the wall as a consequence of the no-slip condition. Incorporating this in (7) and performing a vector premultiplication with $(-\hat{\underset{\sim}{k}})$ gives

$$-\hat{\underset{\sim}{k}}\times\left\{\frac{d\underset{\sim}{v}_0}{dt}+\frac{1}{\rho_0}(grad\,p)_0\right\}-\frac{1}{\rho_0}\begin{bmatrix}\dfrac{\partial\sigma_1}{\partial y}\\ 0\\ 0\end{bmatrix}_0+\frac{1}{\rho_0}\hat{\underset{\sim}{k}}\left\{(curl\,\underset{\sim}{\tau}_0)\cdot\hat{\underset{\sim}{k}}\right\}$$

$$= \frac{1}{\rho_0}\begin{bmatrix}-\dfrac{\partial\tau_{yz}}{\partial z}\\ \dfrac{\partial\tau_{xz}}{\partial z}\\ \dfrac{\partial\tau_{yz}}{\partial x}-\dfrac{\partial\tau_{xz}}{\partial y}\end{bmatrix}_0 \qquad (8)$$

The last term on the left was added to supply the z-component on the right. $\underset{\sim}{\tau}_0$ is the tangential stress at the wall

$$\begin{bmatrix}\tau_{xz}\\ \tau_{yz}\\ 0\end{bmatrix}$$

Comparing (8) with (6), it follows that

$$\underset{\approx}{J}_0\cdot\hat{\underset{\sim}{k}} = \frac{1}{\rho_0}curl\,(\underset{\approx}{S}_0\cdot\hat{\underset{\sim}{k}})$$

$$= \frac{1}{\rho_0}\begin{bmatrix}\dfrac{\partial(\sigma_2-\sigma_1)}{\partial y}\\ -\dfrac{\partial\sigma_2}{\partial x}\\ 0\end{bmatrix}_0 - \hat{\underset{\sim}{k}}\times\left\{\frac{d\underset{\sim}{v}_0}{dt}+\frac{1}{\rho_0}(grad\,p)_0\right\}$$

$$+\frac{1}{\rho_0}\hat{\underset{\sim}{k}}\left\{(curl\,\underset{\sim}{\tau}_0)\cdot\hat{\underset{\sim}{k}}\right\} \qquad (9)$$

The middle term on the right recovers Morton's expression, equation (1), without any assumptions about material behavior. That this is likely, might have been recognized by Morton, Lighthill (1967) and Wu et al., from the disappearance of the kinematic viscosity in their derivation.

The last term on the right is associated with the transport of the wall-normal component of vorticity. This may differ from zero in three-dimensional flows (see also Wu et al.).

The first term on the right arises from wall-parallel components of gradients of the normal-stress differences. Though these occur as consequences of a class of material behavior, the manner in which the material behavior produces them (the constitutive equation) does not influence the form of the expression. The present derivation therefore yields the important new result that the vorticity source strength (9) at a wall is largely independent of material properties.

A fourth term needs to be added to the right side of (9) for three-dimensional flows in which the wall is curved in a plane normal to the wall shear stress $\underset{\sim}{\tau}_0$. This term is

$$\frac{1}{\rho_0}grad\,\hat{\underset{\sim}{n}}\cdot(\hat{\underset{\sim}{n}}\times\underset{\sim}{\tau}_0), \qquad (10)$$

see Wu et al. Here $\hat{\underset{\sim}{n}}$ is to be understood as the wall-normal unit vector. In the present derivation, grad $\hat{\underset{\sim}{n}}$ was presumed to be zero (plane wall) for simplicity.

3. THE VORTICITY TRANSPORT

Once vorticity is generated at a boundary, it can be transported by diffusion and convection into the flow field. In the immediate vicinity of the boundary, the convective transport vanishes because of the no-slip condition, and diffusion is first required to move the vorticity to regions of finite velocity before the convective transport can become effective.

At this point it is important to realize that vorticity need not be generated at the boundaries. For example, density gradients not aligned with pressure gradients lead to finite "baroclinic torque". Irrotational body forces are a further possible distributed source of vorticity. However, if the fluid is not subjected to a net external torque, the net vorticity change must be zero, and vorticity is only generated in equal and opposite amounts no matter whether it occurs at a wall or within the flow field.

These points may be seen more clearly if the curl of the momentum equation

$$\frac{D\underset{\sim}{v}}{Dt} = \frac{1}{\rho}div\,\underset{\approx}{S}+\underset{\sim}{f} \qquad (11)$$

is formed to produce the vorticity transport equation

$$\rho\frac{D\,(\underset{\sim}{\omega}/\rho)}{Dt}-(grad\,\underset{\sim}{v})\cdot\underset{\sim}{\omega}$$

$$= \frac{1}{\rho}curl\;div\,\underset{\approx}{S}+grad\frac{1}{\rho}\times div\,\underset{\approx}{S}+curl\,\underset{\sim}{f}. \qquad (12)$$

Here $\underset{\sim}{f}$ is the specific body force, whose curl may be seen from (10) to contribute changes of vorticity. The other two terms on the right represent the diffusive transport and the baroclinic torque. The second term on the left is due to that contribution to the rate of change of angular velocity which arises from the stretching of vortex lines.

It is interesting to discuss the form of (11) and (12) at a non-accelerating no-slip boundary in the absence of body forces, when (11) degenerates to

$$(div \underset{\approx}{S})_0 = 0, \tag{13}$$

and, since $(grad\, v)_0$ is then also zero, (12) degenerates to

$$\left[\rho \frac{D(\underset{\sim}{\omega}/\rho)}{Dt}\right]_0 = \frac{1}{\rho_0}(curl\ div\ \underset{\approx}{S})_0. \tag{14}$$

I.e., the baroclinic torque is zero at a non-accelerating no-slip boundary.

In order to illustrate the convective and diffusive transport, consider the special situation of constant-density Newtonian flow, for which

$$\underset{\approx}{R} = 2\rho\nu\underset{\approx}{D},$$

where

$$\underset{\approx}{D} = \frac{1}{2}\left(\frac{\partial v_i}{\partial x_j} + \frac{\partial v_j}{\partial x_i}\right)$$

in indicial notation, and ν is the kinematic viscosity, so that (11) and (12) become

$$\frac{D\underset{\sim}{v}}{Dt} = -\frac{1}{\rho} grad\, p + \nu\, div\ grad\, \underset{\sim}{v} \tag{15}$$

and

$$\frac{D\underset{\sim}{\omega}}{Dt} - (grad\, \underset{\sim}{v})\cdot\underset{\sim}{\omega} = \nu\, div\ grad\, \underset{\sim}{\omega} \tag{16}$$

To simplify the illustration further proceed to text-book land, where the world is plane, and vorticity becomes a scalar, having only the y-component if the flow plane is chosen to be the (zx)-plane. The stretching term then vanishes, and

$$\frac{D\omega}{Dt} = \nu\, div\ grad\, \omega. \tag{17}$$

Consider first the simple case of steady laminar channel flow see Fig. 1. Here grad $p = dp/dx$ is a negative constant, the velocity profile is parabolic, $grad\, \omega = d\omega/dz$ is a negative constant, and lines of constant vorticity are parallel to the x-axis. Hence the diffusive vorticity transport (down the vorticity gradient) goes straight from one wall across to the other, see Fig. 1.

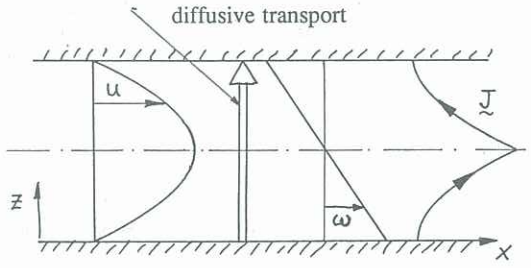

Fig. 1 Vorticity transport in channel flow. (Sketch only)

To the diffusive transport the convective transport must be added to obtain the local vorticity transport vector. This occurs in the direction of $\underset{\sim}{v}$ if ω is positive and in the direction of $(-\underset{\sim}{v})$ if ω is negative. In the example of the channel flow, the convective transport therefore changes discontinuously at the center of the channel, and disappears at the walls. The resulting line of vorticity transport (parallel to the local direction of vorticity transport) is as shown in Fig. 1, making a kink with finite angle at the centerline.

Some students find it difficult to accept this way of looking at vorticity transport, because they feel that convection can convey only in the direction of $\underset{\sim}{v}$. This is certainly true of a quantity that can only be positive. However, the convention adopted here is that convection of a negative quantity downstream is equivalent to transport of the positive quantity upstream. As will be seen later, this gives the vorticity transport field the appropriate symmetry without making it necessary to discuss positive and negative vorticity separately.

In this convention the vorticity transport field lines usually form a kink where they cross lines of zero vorticity.

Now consider the case of external flow, for example over a circular cylinder, at different Reynolds numbers, starting with the creeping flow at Re→ 0. This is a particularly simple case because the lines of constant ω have fore-and-aft symmetry and the convective transport may be neglected compared with the diffusive transport, see Fig. 2. It follows that the $\underset{\sim}{J}$-field, which (in the absence of convection) is everywhere normal to the lines of constant ω, also has fore-and-aft symmetry. All the vorticity generated in the upper half at the cylinder surface flows through the stagnation streamline and back into the body in the lower half, in equal amounts in front of and behind the body. A $\underset{\sim}{J}$-field line leaving the surface signifies generation of positive vorticity, and a $\underset{\sim}{J}$-field line entering the body signifies destruction of positive vorticity (equivalent to generation of negative vorticity). Note that no net vorticity is produced, consistently with the absence of an external torque.

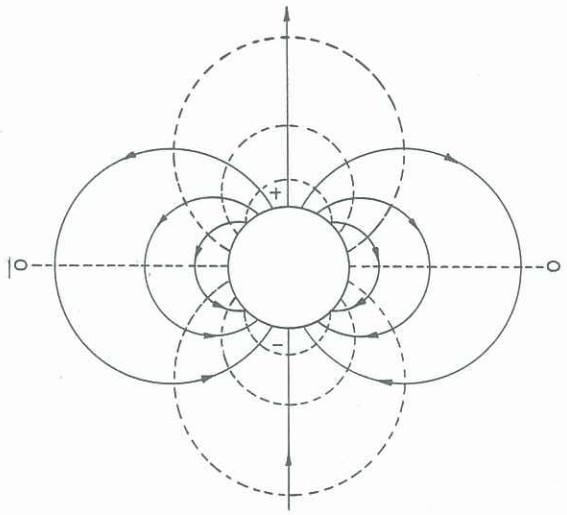

Fig. 2 Lines of constant vorticity (dashed) and lines of vorticity transport (full lines with arrowheads) for creeping flow over a circular cylinder Re → 0. (Sketch only)

Now add a small amount of convection by increasing the Reynolds number to 4. (For this purpose and the higher Reynolds number, it is convenient to use the results of Apelt (1961) and Keller and Takami (1966) as given by Batchelor (1967).) The flow field loses its fore-and-aft symmetry, see Fig. 3. The vorticity maximum is moved upstream from its mid position, and consequently the division between the transport through the rear stagnation line and the transport through the upstream stagnation line is also moved upstream. This is because, at the wall, the $\underset{\sim}{J}$-field lines must be orthogonal to the lines of constant ω. Also, some of the $\underset{\sim}{J}$-field lines leaving the body from the upper half reenter it in the upper half. The $\underset{\sim}{J}$-field lines form kinks at the symmetry plane ($\omega = 0$) which point in the local $\underset{\sim}{v}$-direction.

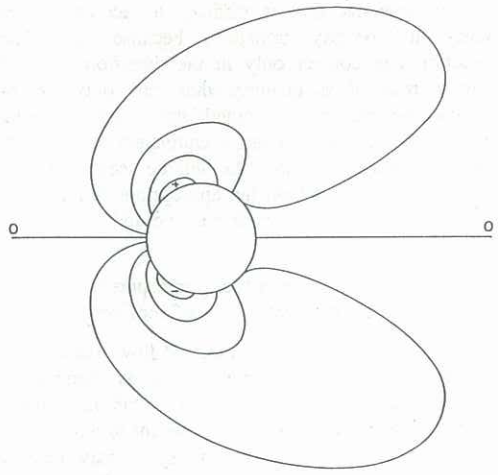

Fig. 3a Lines of constant vorticity, Re = 4. After Keller and Takami, taken from Batchelor.

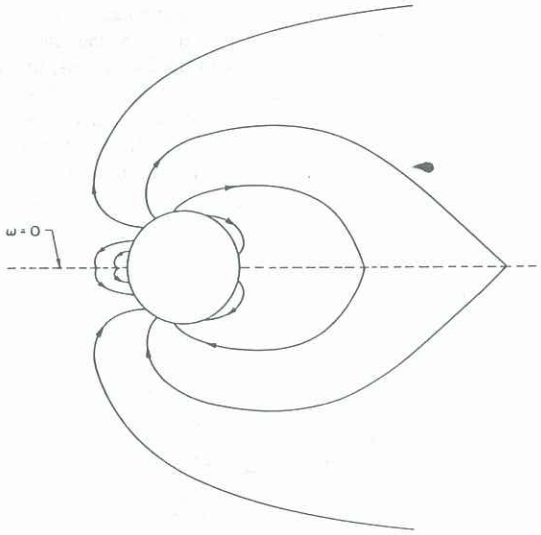

Fig. 3b Lines of vorticity transport, Re = 4. (Sketch only)

Now add still more convection by increasing the Reynolds number to 40. This causes both a separation to appear, and a new line of zero vorticity to leave the body and cross the rear stagnation streamline, see Fig. 4. The lobes formed by the lines of constant vorticity are further elongated in the downstream direction. The $\underline{J}$-field lines may be constructed by aligning them with $(-grad\,\omega)$ at the wall and by the kink where they cross a line of zero vorticity pointing in the direction of $\underline{v}$. Note the special case of the saddle point formed by the lines of constant ω on the rear stagnation streamline.

No further qualitative change occurs in the lines of constant ω or in the J-field lines with further increase of Reynolds number (assuming the flow to remain steady). The qualitative features of Fig. 4 also apply to a large class of other bodies. For example, the $\underline{J}$-field lines on a lifting airfoil with separation are sketched in Fig. 5 and are seen to be topologically the same as those of Fig. 4.

The two simple rules used here for constructing the $\underline{J}$-field lines in two-dimensional flows are not simply extendible to each of the components of $\underline{\omega}$ in the case of three-dimensional or axially symmetric flow. This is because of the fact that the stretching term does not vanish. They do apply in plane unsteady flow, however.

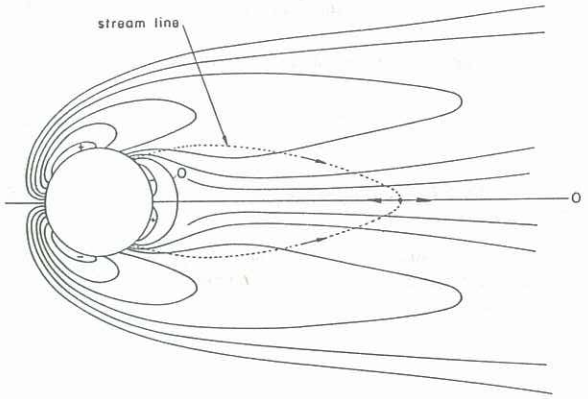

Fig. 4a Lines of constant vorticity, Re = 40. After Apelt, taken from Batchelor.

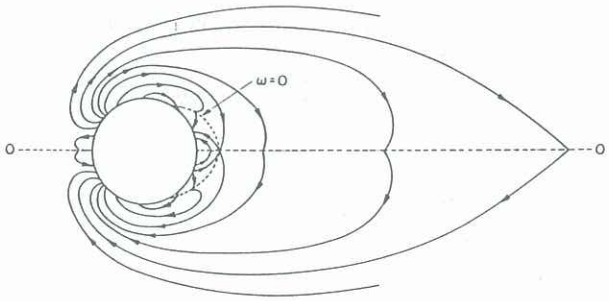

Fig. 4b Lines of vorticity transport, Re = 40. (Sketch only)

4. EXAMPLES

The vorticity source strength at a wall, applied to plane steady flow over a flat plate with a rounded leading edge, gives the well-known result that all the vorticity is generated near the leading edge of the plate, because this is the only region where the pressure gradient is significant. Another well-known example is flow resulting from the impulsive acceleration of a flat wall from rest to a constant velocity parallel to the wall, in which all the vorticity is generated at the instant of acceleration at the wall. These results are reiterated here only to point out that the flow does not have to be Newtonian for them to be true.

Vortex Near a Wall

Massive transport of vorticity away from a wall to distances that are large compared with the boundary layer thickness may occur when convective transport becomes active close to the wall. This is precisely what happens at separation, because the vorticity generated upstream and conveyed by the boundary layer is shaved off by convective transport with a component normal to the wall. This is also the mechanism by which a vortex swimming over a flat-plate boundary layer may cause vorticity to be convected away from the wall.

Consider a vortex of circulation Γ located a distance h above a flat plate in plane steady Newtonian flow at constant density. The pressure change at the plate caused by the presence of the vortex may be obtained approximately by the method of images to be

$$\Delta p = \frac{\rho U \Gamma}{h} \cdot \frac{1}{1+(x^2/h^2)},$$

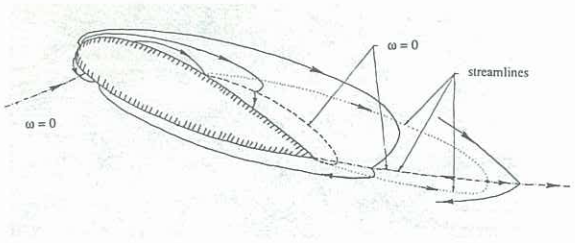

Fig. 5 Flow over a lifting airfoil showing topological similarity to flow over circular cylinder.

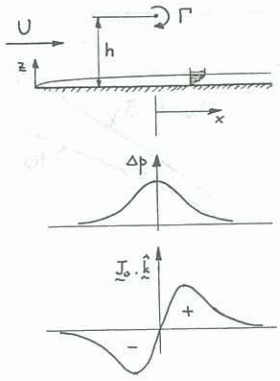

Fig. 6 Vortex over a flat plate boundary layer showing pressure distribution and vorticity source strength for weak vortex (sketch only).

where U is the free-stream speed and x is measured along the flat plate from an origin directly under the vortex, see Fig. 6. Hence equation (9) gives

$$\underset{\sim}{J}_0 \cdot \hat{\underset{\sim}{k}} = \frac{1}{\rho_0} grad\, p_0 = \frac{U\Gamma}{\pi h^3} \frac{2x}{(1+x^2/h^2)^2}. \qquad (18)$$

This is also sketched in Fig. 6. As may be seen, an upstream area of negative vorticity production is followed by a downstream area of positive vorticity production and no net vorticity is produced. If, however, $U\Gamma/h^2$ is sufficiently large, the pressure gradient may be strong enough to cause separation, or, in other words, the negative vorticity production rate may be fast enough to cause the wall vorticity to drop to zero, see Fig. 7. If this happens, practically no additional vorticity production occurs downstream of this point, because the pressure gradient under the separated flow is very small. Thus, a sufficiently strong vortex close to the wall may extract a new vortex from the wall through the mechanism of separation.

Now extend this to the three-dimensional case of a strong oblique vortex over a flat plate. It is easy to see that the wall shear stress field (wall streamlines) will display the pattern shown in Fig. 8. If, in addition, the distance h varies along the length of the vortex as shown in Fig. 9, the wall streamline pattern (also shown in Fig. 9) discussed by Perry and Hornung (1984) results.

This somewhat abstract example has relevance to turbulent boundary layers, which may be characterized approximately as a complex unsteady arrangement of vortices in mainly inviscid flow above a viscous sublayer close to the wall. The vortices may be strong enough to extract new vortices from the wall by causing the sublayer to separate. Thus, the pattern of wall streamlines that might be expected under a strong hairpin vortex is as shown in Fig. 10.

It is interesting to observe that the numerical computation of turbulent boundary layer flow by Moin and Spalart (1987)

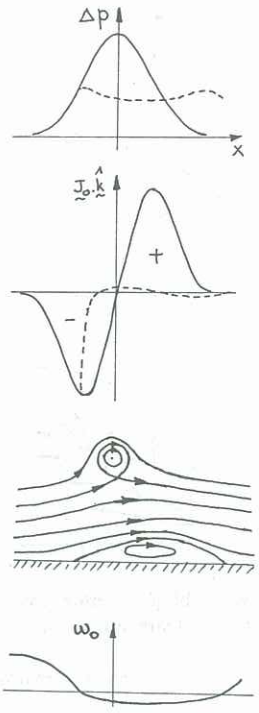

Fig. 7 Vortex over a flat plate boundary layer showing pressure distribution and vorticity source strength for a stronger vortex that produces separation (sketch only).

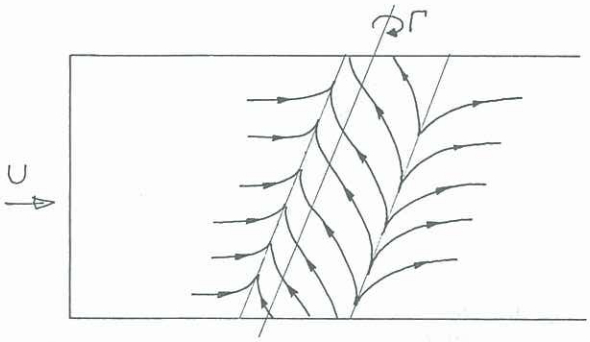

Fig. 8 Oblique strong vortex over a flat plate showing wall streamline pattern (sketch only).

(direct simulation of the Navier-Stokes equations) displays many such structures in the wall streamline pattern, see Fig. 11.

Baroclinic Vorticity Generation by Shock Waves

At locations other than the wall, the baroclinic torque $grad\,(1/\rho) \times div\, \underset{\approx}{S}$ in equation (12) is a possible source of vorticity in flows with variable density. In the regions where this baroclinic torque is active, $div\, \underset{\approx}{S}$ often (but not always) degenerates to $(-grad\, p)$. Thus, the baroclinic torque is finite if pressure gradient and density gradient are not aligned. In steady flows, such a situation may arise within a curved shock wave. An elegant derivation for the vorticity after a curved shock ω_2 is given by Hayes and Probstein (1959). It leads to

$$\omega_2 = \frac{U}{r} \frac{(1-\varepsilon)^2}{\varepsilon} \cos\beta, \qquad (19)$$

where U is the free-stream speed, r is the radius of curvature of the shock, ε is the inverse density ratio across the shock, and β is the shock angle. For a shock wave of hyperbolic shape with a finite radius of curvature r_0 at the front and

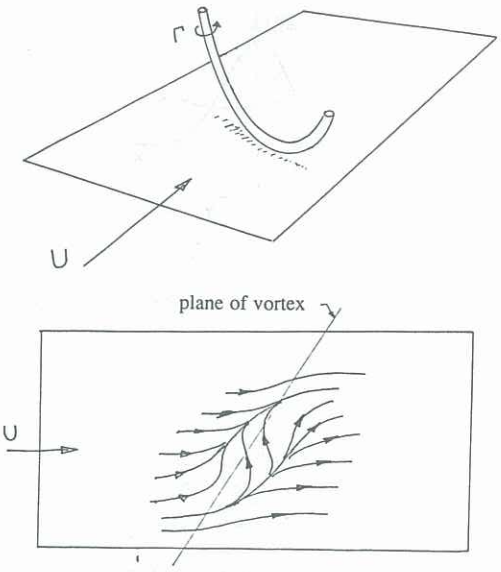

Fig. 9 a) Curved oblique vortex over a flat plate. b) Associated wall streamline pattern. (Sketch only)

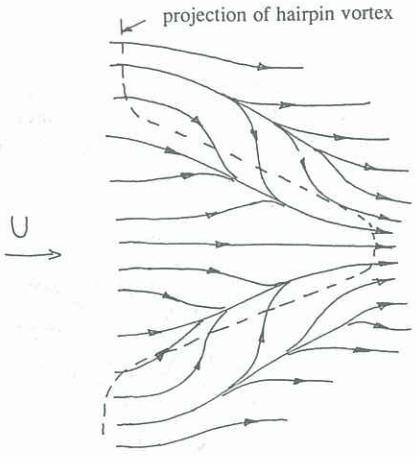

Fig. 10 Wall streamline pattern under a strong hairpin vortex (sketch only).

asymptoting to the Mach angle far downstream, Fig. 12 shows the distribution of ω_2 over the shock angle for a diatomic gas at Mach number 4 and 10. Clearly, $\omega_2 = 0$ at $\beta = \pi/2$ and at the Mach angle, and a maximum occurs somewhere between these values. This maximum increases rapidly with Mach number and typically produces vorticity comparable with that in the boundary layer at Mach numbers around 10. The vorticity distribution at the shock is carried downstream unchanged in the inviscid part of the flow (convective transport only) because the flow along streamlines is isentropic and therefore the baroclinic torque vanishes. Hence the vorticity maximum is eventually "swallowed" by the boundary layer. Since a vorticity distribution with a maximum is dynamically unstable, this may influence the stability of the boundary layer and cause early transition, see Stetson et al.(1984). Some control over this effect may be exercised through the choice of the nose radius of curvature of a blunt body generating such a shock.

A second example under this heading is that where a shock wave traverses an interface between fluids at different densities. Consider a circular cylinder of gas A surrounded by gas B at a different density. Let a plane shock wave whose front is parallel to the axis of the cylinder, traverse the

Fig. 11 Wall streamline pattern in a turbulent wall flow computed by Moin and Spalart.

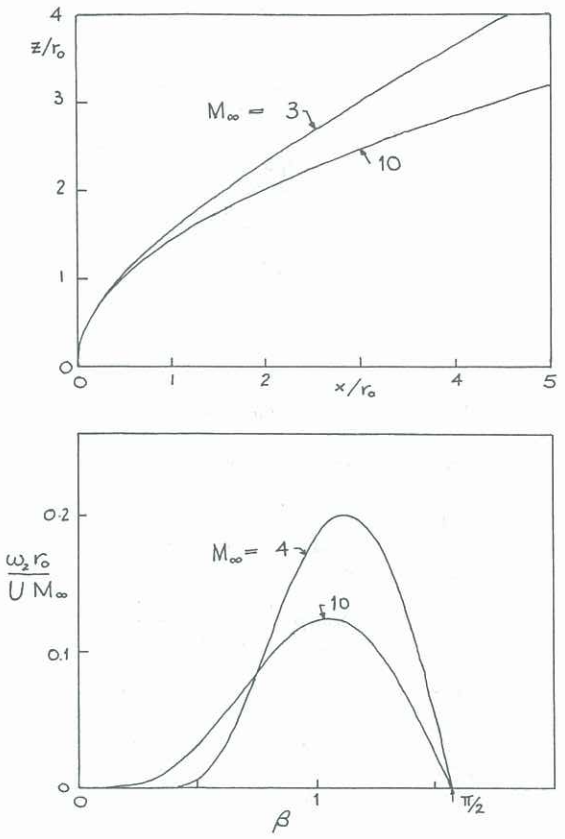

Fig. 12 Vorticity produced by the baroclinic torque in a curved shock. (Assumed shock shape is a hyperbola with Mach angle as downstream asymptote.) a) Shock shape for Mach numbers 3 and 10. b) Vorticity distribution over shock angle for Mach numbers 4 and 10.

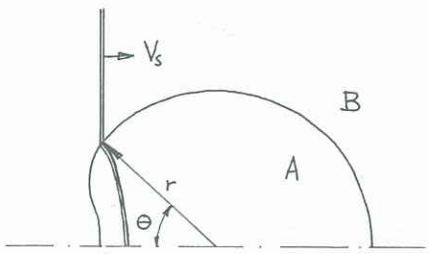

Fig. 13 Shock wave traversing circular cylinder of different-density gas. Schematic for gas A lighter than gas B.

cylinder, see Fig. 13. The circulation generated on one side of the cylinder by the baroclinic torque may be crudely estimated as follows: Let the interface between the two gases have density difference $\Delta\rho$ and thickness δ_1. Let the pressure difference across the shock wave be Δp and let its thickness be δ_2. Then

$$grad\frac{1}{\rho} \times grad p \approx \frac{\Delta p\,\Delta\rho}{\delta_1\delta_2} \cdot \frac{1}{\rho^2} \sin\theta$$

is the rate of vorticity production in the area of intersection between shock and interface. In a time

$$dt = \frac{r \sin\theta}{V_s} d\theta$$

the circulation produced is

$$d\Gamma = d\omega \cdot \text{area} \approx \frac{\Delta p\,\Delta\rho}{\delta_1\delta_2} \cdot \frac{1}{\rho^2} \sin\theta \cdot \frac{r \sin\theta d\theta}{V_s} \cdot \frac{\delta_1\delta_2}{\sin\theta}$$

Hence,

$$\Gamma \approx \frac{\Delta p\,\Delta\rho}{\rho^2 V_s} r \int_0^{\pi} \sin\theta\, d\theta,$$

$$\Gamma \approx \frac{2\Delta p\,\Delta\rho}{\rho^2 V_s} r. \qquad (20)$$

(Other authors have given more accurate estimates and numerical computations.) Thus, a pair of line vortices of equal and opposite circulation is produced, the order of magnitude of which is given by equation (20). Of course, this can only be a crude estimate, because complex secondary interactions between diffracted shock waves with interfaces and between each other also create vorticity through the baroclinic torque, apart from the approximations inherent in the above.

A recent experiment by Jacobs (1989), in which a laminar circular helium jet blowing across a shock tube containing air was traversed by a shock, demonstrates this mechanism dramatically. Earlier experiments by Haas and Sturtevant (1987) in which gas A was contained by a soap film or a very thin membrane with a great variety of the parameters also show the various stages of development during the process.

The baroclinic torque is clearly an important mechanism in compressible turbulent flows. It is the dominant process in supersonic mixing.

5. CONCLUSIONS

The expression for the vorticity source strength at a solid wall bounding a fluid, which had previously been derived by assuming the flow to be Newtonian, was shown to be largely independent of material properties. Some features of the vorticity transport field were obtained by considering the simple case of plane Newtonian flow. Examples relevant to wall turbulence and to compressible flow were used to illustrate generation mechanisms.

6. REFERENCES

APELT, C. J. (1961) Aero. Res. Coun., Rep. and Mem. no. 3175.

BATCHELOR, G. K. (1967) An Introduction to Fluid Dynamics, Cambridge University Press: London.

HAAS, J.-F. & STURTEVANT, B. (1987) Interaction of weak shock waves with cylindrical and spherical gas inhomogeneities. J. Fluid Mechanics, 181, pp. 41-76.

HAYES, W. D. & PROBSTEIN, R. F. (1959) Hypersonic Flow Theory, Academic Press: New York.

JACOBS, J. (1989) Shock-induced mixing inhomogeneities. In preparation.

KELLER, H. B. & TAKAMI, H. (1966) Proc. Symposium on Numerical Solution of Nonlinear Differential Equations, University of Wisconsin.

LIGHTHILL, M. J. (1967) Introduction, Boundary Layer Theory, in Laminar Boundary Layers, ed. L. Rosenhead, Oxford University Press.

MOIN, P. & SPALART, P. R. (1987) Contributions of Numerical Simulation Data Bases to the Physics, Modeling and Measurement of Turbulence, NASA TM 1000022.

MORTON, B. (1984) The generation and decay of vorticity. Geophysical and Astrophysical Fluid Dynamics, 28, p. 277.

PERRY, A. E. & HORNUNG, H. G. (1984) Some aspects of three-dimensional separation, Part II: Vortex skeletons. Z. Flugwiss. Weltraumf. 8, pp. 155-160.

STETSON, K.F., THOMPSON, E.R., DONALDSON, J.C. & SILER, L. G. (1984) Laminar Boundary Layer Stability Experiments on a Cone at Mach 8, Part 2: Blunt Cone. AIAA paper AIAA-84-0006.

WU, J. Z., WU, J. M. & WU, C. J. (1987) A general 3-D viscous compressible theory on the interaction of solid body and vorticity-dilatation field. UTSI report 87/03.